JOURNAL OF PETROLOGY | VOLUME 40 | NUMBER 3 | PAGES 363–380 | 1999

Assimilation of Crustal Xenoliths in a Basaltic Magma Chamber: Sr and Nd Isotopic Constraints from the Hasvik Layered Intrusion, Norway

C. TEGNER[1]*, B. ROBINS[2], H. REGINIUSSEN[3] AND S. GRUNDVIG[1]

[4]DEPARTMENT OF EARTH SCIENCES, C.F. MØLLERS ALLE, UNIVERSITY OF AARHUS, 8000 AARHUS C, DENMARK

[2]DEPARTMENT OF GEOLOGY, ALLÉGT. 41, 5007 UNIVERSITY OF BERGEN, NORWAY

[3] NORDIC VOLCANOLOGICAL INSTITUTE, GRENSASVEGUR 50, 108 REYKJAVIK, ICELAND

RECEIVED DECEMBER 3, 1996; REVISED TYPESCRIPT ACCEPTED JULY 1, 1998

Strontium and neodymium isotopic data for mafic cumulates, chilled margins, and adjacent crustal rocks of the Hasvik Layered Intrusion, North Norwegian Caledonides, are reported together with new mineralogical and whole-rock analytical data to constrain the extent and effect of the assimilation of crustal xenoliths in a basaltic magma chamber. Initial $^{87}Sr/^{86}Sr$ (700 Ma) of 0·7045 and ε_{Nd} (700 Ma) of +3·03 for the chilled margin, which has a tholeiitic composition akin to the chilled rocks of the Skaergaard intrusion, demonstrate that the parental magma was derived from a depleted mantle source. The basal cumulates (0–335 m) show an up-section decrease in $^{87}Sr/^{86}Sr$ from 0·7045 to 0·7038 and a correlative increase in ε_{Nd} from +1·82 to +4·26 suggesting mixing between resident and recharging magma during magma chamber expansion. The overlying fractionated cumulate sequence (335–1550 m) shows an uninterrupted tholeiitic crystallization sequence (olivine out, orthopyroxene in, Fe–Ti oxides in, and apatite in) accompanied by a remarkably smooth up-section increase in $^{87}Sr/^{86}Sr$ from 0·7038 to 0·7089, correlated with decreasing ε_{Nd} (+4·76 to –3·26), decreasing whole-rock mg*-number (0·73–0·30), and changing mineral compositions (e.g. the anorthite component of plagioclase decreases from 0·72 to 0·52). These compositional variations point to steady-state assimilation of crustal rocks accompanied by fractional crystallization (AFC). AFC modelling based on the Sr and Nd isotopic data demonstrates that the rate of assimilation relative to the rate of crystallization was constant at ~0·27. The amount of assimilated crust, ~21% in bulk for the fractionated cumulate section, is close to the upper limit permitted by the thermal budget and places the Hasvik Layered Intrusion among the most contaminated layered intrusions known. Thousands of recrystallized tabular xenoliths of metasedimentary origin enclosed in the cumulates are thought to represent the remnants of the assimilated material. The xenoliths spalled off the roof during magma emplacement, and, together with the elevated temperatures (400–600°C) of the mid-crustal country rocks, led to a high degree of assimilation in the Hasvik magma chamber.*

KEY WORDS: *layered intrusion; Hasvik; strontium and neodymium isotopes; crustal assimilation; fractional crystallization*

INTRODUCTION

Crustal contamination of mantle-derived magmas mainly takes place in large magma chambers. This is the consequence of the release of latent heat of crystallization (Bowen, 1928; Wilcox, 1954; DePaolo, 1981) and the long magma residence time in crustal magma chambers. Layered mafic intrusions, in which the cumulates record a history of complex magma chamber processes such as fractional crystallization, replenishment, venting, convection, stratification and contamination, provide important constraints on the degree and physical processes of crustal assimilation, the crystallization sequence, and

*Corresponding author. Telephone: (+45) 89 42 25 08. Fax: (+45) 89 42 25 25. e-mail: christian.tegner@geo.aau.dk

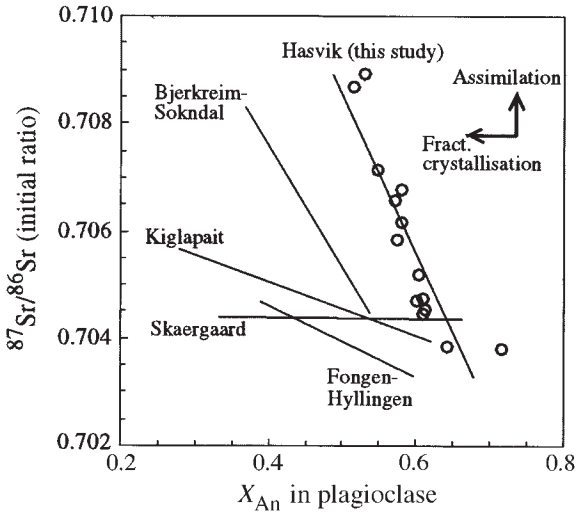

Fig. 1. Correlation of initial $^{87}Sr/^{86}Sr$ and X_{An} in plagioclase in studied layered intrusions where coupled assimilation and fractional crystallization have been suggested. Shown are regression lines through data for Kiglapait (DePaolo, 1985), Skaergaard (Stewart & DePaolo, 1990), Fongen–Hyllingen (Sørensen & Wilson, 1995) and Bjerkreim–Sokndal (Nielsen *et al.*, 1996). Also shown are the data discussed in this study obtained from the Hasvik Layered Intrusion (only cumulates in a fractionated sequence between ~335 and 1550 m stratigraphic height are shown).

the liquid line of descent of mantle-derived magmas. Enigmatic questions include the nature of the assimilated material (wall or roof rocks, xenoliths and/or partial melts), where and when in the magma chamber assimilation took place, the amount of assimilation, the amount of heat available, and the relation to fractional crystallization. These factors will vary with the magma temperature and composition, depth and mechanisms of magma emplacement, shape of the magma chamber, mode of cooling and convection, and lithology, structure and temperature of the country rocks.

A marked correlation between mineral compositions and initial isotopic ratios has been demonstrated in several layered intrusions, e.g. Kiglapait (DePaolo, 1985), Fongen–Hyllingen (Sørensen & Wilson, 1995) and Bjerkreim–Sokndal (Nielsen *et al.*, 1996) (Fig. 1), suggesting concurrent assimilation and fractional crystallization (AFC). For these intrusions the researchers call upon physical and/or diffusional entrainment of contaminants across a boundary layer separating the basaltic magma reservoir from an overlying layer of buoyant, anatectic crustal melt residing at the roof of the chamber. The preservation of distinct mafic and felsic layers in large plutons indicates, however, that the amount of material exchange between crustal granophyre and basalt is either negligible (Geist & White, 1994) or restricted chiefly to the effect of diffusion, in particular isotopic self-diffusion (Lesher, 1990, 1994; Blichert-Toft *et al.*, 1992; Stewart & DePaolo, 1992, 1996).

Here we present evidence for the assimilation of crustal xenoliths in the tholeiitic Hasvik Layered Intrusion (HLI), which was emplaced into the middle crust at 6–7·5 kbar and forms part of the Seiland Igneous Province within the North Norwegian Caledonides. This particular study was initiated because the abundance of recrystallized metasedimentary xenoliths suggested very high extents of crustal contamination in a tholeiitic cumulate sequence that otherwise is reminiscent of the Skaergaard intrusion (Robins & Gardner, 1974; Gardner, 1980; Robins, 1985). We collected 40 new samples from a profile through the ~1550 m thick cumulate sequence, the chilled mafic rocks and the adjacent metasedimentary country rocks, and report here new mineralogical, bulk-rock and Sr–Nd isotopic data. This study aims to revise the stratigraphic systematics in the layered cumulates, and to constrain the extent and physical processes of assimilation in a crustal magma chamber enclosing abundant country-rock xenoliths.

GEOLOGICAL BACKGROUND

The HLI is part of the Late Proterozoic–Middle Cambrian Seiland Igneous Province exposed within the Sørøy–Seiland Nappe, the uppermost tectonic unit of the Kalak nappe complex that forms the Middle Allochthon of the North Norwegian Caledonides (Fig. 2). The Seiland Igneous Province comprises a voluminous suite of plutonic rocks with a wide compositional range including gabbros, ultramafic rocks, syenites, nepheline syenites and carbonatites (Robins & Gardner, 1975). Radiometric dating suggests that emplacement of mantle-derived magmas occurred episodically between ~830 Ma and ~520 Ma (Pedersen *et al.*, 1989; Krogh & Elvevold, 1990; Daly *et al.*, 1991), i.e. long before the emplacement of the Caledonian nappes at ~425–400 Ma (Dallmeyer *et al.*, 1988). The detailed tectonic and magmatic history of the Sørøy–Seiland Nappe is enigmatic, partly because of a dearth of precise radiometric ages for the various intrusions. Most recent workers, however, have suggested that magmatism was associated with the crustal extension that eventually led to continental breakup and opening of the Iapetus Ocean (Krill & Zwaan, 1987; Daly *et al.*, 1991; Reginiussen *et al.*, 1995).

THE HASVIK LAYERED INTRUSION

Exposures of the HLI occupy ~12 km^2 on the southwestern tip of the island of Sørøy, Finnmark (Figs 2 and 3). The emplacement of the HLI has been dated to 700 $\pm$ 33 Ma on the basis of two internal Sm–Nd mineral/whole-rock isochrons (Daly *et al.*, 1991). The HLI was emplaced into the vertical to overturned limb of a large, pre-existing, east-verging antiform in the country rocks

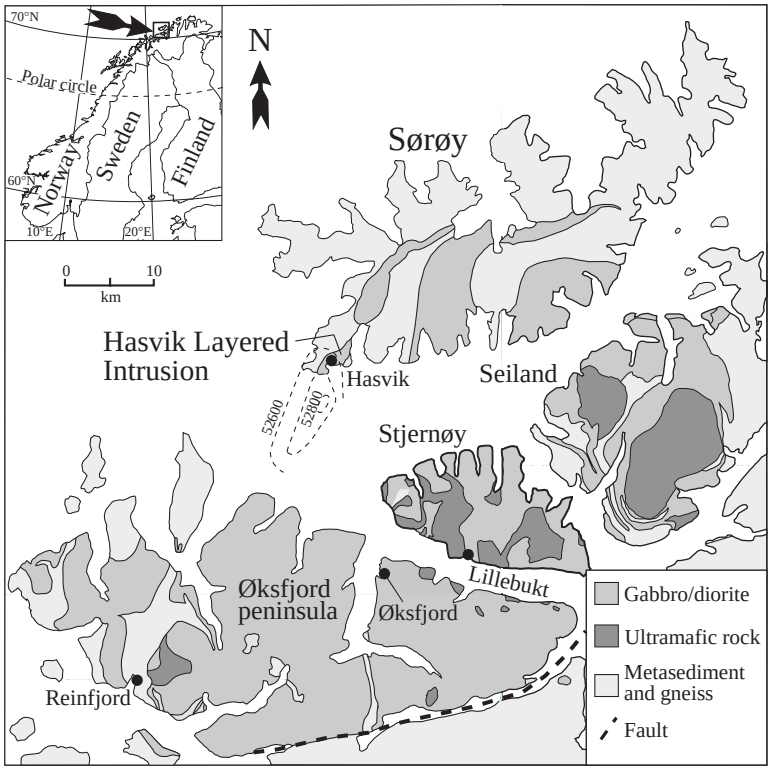

Fig. 2. Geological map of the Sørøy–Seiland nappe showing the Late Proterozoic–Middle Cambrian Seiland Igneous Province and the location of the studied ~700 Ma old Hasvik Layered Intrusion. A large positive aeromagnetic anomaly immediately SSW of the study area, shown by the stippled contours of gamma value (Roberts, 1974), suggests that the exposure of the HLI is only the northern end of a much larger pluton extending >10 km south-westward beneath the Lopphavet sea.

(Sturt, 1969; Robins & Gardner, 1974). In the south, the HLI has a wedge-shaped cross-section, narrowing downwards (Fig. 3). When followed northwards, the almost vertical western contact takes up a steep outward-dipping orientation and eventually a moderately north-westward dip where the intrusion pinches out to the north. The exposure on Sørøy is probably only the end of a much larger pluton extending SSW beneath the sea, as indicated by a large aeromagnetic anomaly shown in Fig. 2. Layering and mineral laminations in the HLI define an upright, asymmetrical syncline with a SW-plunging axis. This may well be a primary feature of the intrusion, but the steep orientation of the layering in the limbs of the syncline suggests that it has been accentuated by later deformation.

Marginal and Upper Border Series

The cumulates have been subdivided into a narrow Marginal Border Series, a Layered Series and an Upper Border Series that crystallized respectively on the wall, floor and roof of the magma chamber (Fig. 3) (Robins & Gardner, 1974; Gardner, 1980; Robins, 1985). The Marginal Border Series is up to 100 m thick along the western contact of the HLI and consists of a thin, outer zone of hybrid gabbro with abundant crustal xenoliths, followed inwards by homogeneous, fine-grained, sub-ophitic olivine gabbro. Further inwards, the marginal gabbro is coarser grained and locally banded. The Upper Border Series is preserved only as a flat-lying ~60 m thick cap on a mountain top (Fig. 3); it consists of massive oxide gabbro–norite (plagioclase–orthopyroxene–augite–Fe–Ti oxide cumulate) characterized by abundant, large amphibole oikocrysts of primary igneous origin.

Layered Series

The Layered Series as developed along the sampled profile is ~1550 m thick and can be subdivided into four zones defined by distinct cumulus parageneses reflecting the degree of magma differentiation (Fig. 4). In stratigraphic order the zones are as follows.

Basal Zone (BZ)

The BZ is ~75 m thick (stratigraphic height, $H = 0$–75 m) and consists of laminated gabbro–norite (plagioclase–

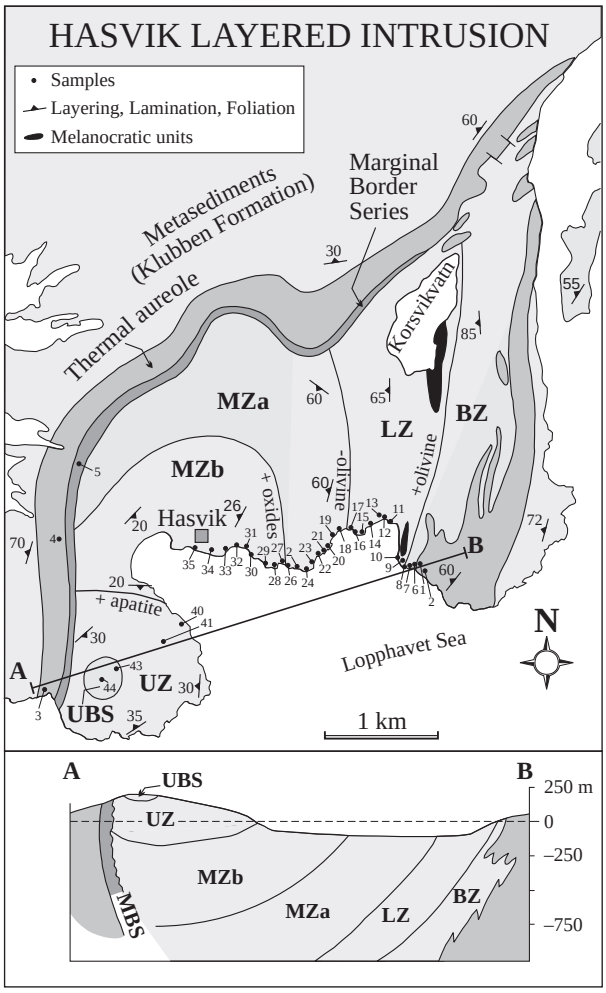

Fig. 3. Geological map and cross-section (no vertical exaggeration) of the Hasvik Layered Intrusion, showing the location of samples. Modified after Gardner (1980) and Robins (1985).

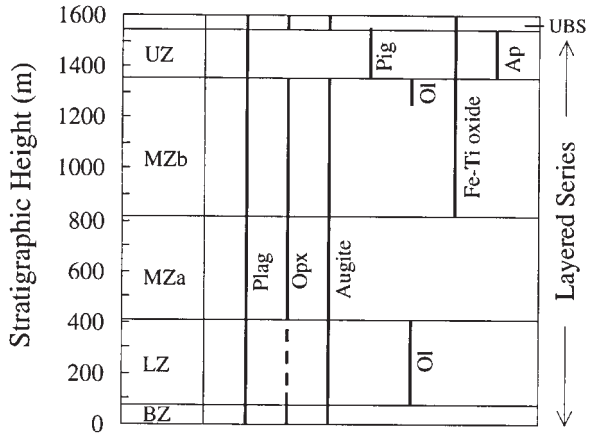

Fig. 4. Stratigraphic section of the Layered Series and the Upper Border Series (UBS) of the Hasvik Layered Intrusion showing the distribution of cumulus minerals (a stippled line indicates sporadic cumulus status), and the zonal subdivision. Plag, plagioclase; Opx, orthopyroxene; Pig, pigeonite; Ol, olivine; Ap, apatite; BZ, Basal Zone; LZ, Lower Zone; MZ, Middle Zone; UZ, Upper Zone.

orthopyroxene–augite cumulate) with patches of gabbro pegmatite. The BZ interdigitates with the contact-metamorphic aureole and contains numerous centimetre-sized xenoliths of highly recrystallized metasediment (see below).

Lower Zone (LZ)

The ~335 m thick LZ (75–410 m) consists of olivine gabbros (plagioclase–augite–olivine cumulate) with rare cumulus orthopyroxene in some samples; the presence of olivine makes the LZ the most primitive cumulate asssemblage in the Layered Series. Modal layering is present in its lower part, which locally contains melanocratic and ultramafic units up to tens of metres thick (Fig. 3).

Middle Zone (MZ)

The ~950 m thick MZ (410–1360 m) consists of gabbro–norite (MZa) and oxide gabbro–norite (MZb). The base of MZa is marked by the disappearance of cumulus olivine and the reappearance of abundant cumulus orthopyroxene. The base of MZb is defined by the first appearance of cumulus Fe–Ti oxides, mainly magnetite and subordinate ilmenite (Robins, 1985). Olivine briefly reappears as a cumulus phase in the upper part of MZb.

Upper Zone (UZ)

The UZ (1360–1550 m) forms the uppermost portion of the Layered Series and consists of oxide–apatite ferronorites (plagioclase–orthopyroxene–Fe–Ti oxide–apatite cumulate) that contain intercumulus quartz and quartz–alkali feldspar intergrowths. The base of the UZ is marked by the entry of cumulus apatite and the disappearance of augite. Pyroxene in the UZ crystallized as pigeonite and inverted during cooling to orthopyroxene with broad exsolution lamellae of augite. Rare augite cores preserved within some pigeonite grains witness early crystallization of augite and its subsequent reaction with the melt.

Country rocks

The HLI was emplaced into migmatitic, banded metasediments of the lowermost unit of the Sørøy Succession (Klubben Formation; Roberts, 1974). Before magma emplacement the metasediments had been metamorphosed, folded and foliated during three phases of regional deformation. The typical mineral assemblage of the country rock is quartz, K-feldspar, plagioclase, garnet, biotite and sillimanite. The metasediments are banded on a decimetre to metre scale and their protoliths were

arkosic sandstones, quartzites, pelites and minor calc-silicates.

Thermal aureole

The HLI has a thermal aureole up to 500 m wide (Fig. 3) (Gardner, 1980). The contact metamorphism has resulted in dehydration and partial-melting reactions which consumed biotite, feldspar and quartz, and produced high-temperature assemblages comprising sillimanite, garnet, orthopyroxene, cordierite, corundum, spinel and K-feldspar. Within the intrusive contact rocks there are abundant centimetre-sized, aluminium-rich and silica-poor lenses composed of highly calcic plagioclase (X_{An} = 0·90) and hercynitic spinel (± corundum and sillimanite), that represent refractory, recrystallized restites of country rock. Agmatites within the thermal aureole imply partial melting during the contact metamorphism. Geothermobarometry based on the garnet–orthopyroxene–plagioclase–quartz equilibrium (Harley, 1984*a*) and aluminium solubility in garnet and orthopyroxene (Harley & Green, 1982) indicates peak temperatures in the inner aureole of at least 875°C (H. Reginiussen & S. Elvevold, unpublished data, 1997). Geobarometry using the garnet–orthopyroxene–plagioclase–quartz equilibrium (Bohlen *et al.*, 1983) and aluminium solubility in orthopyroxene (Harley, 1984*b*) suggests that thermal metamorphism took place at a pressure between 6 and 7·5 kbar (H. Reginiussen & S. Elvevold, unpublished data, 1997). This pressure range is consistent with estimates of 5–7 kbar for metamorphic mineral assemblages in contact aureoles and xenoliths for other gabbro plutons within the Seiland Igneous Province (Elvevold *et al.*, 1994). These pressure estimates suggest the HLI was emplaced at ~20–km depth, corresponding to initial country-rock temperatures of 400–600°C for geothermal gradients between 20°C/km (shield) and 30°C/km (extended crust).

Fig. 5. Examples of country-rock xenoliths in the Layered Series of the Hasvik Layered Intrusion. (a) Numerous thin slivers of recrystallized crustal xenoliths (white–grey flakes) typical of the Middle and Upper Zone. (b) Close-up of recrystallized xenolith in the Middle Zone. (c) Relict folded banding within a large xenolith enclosed in the Upper Zone.

Metasedimentary xenoliths

Xenoliths of recrystallized country rocks are abundant within the cumulates of the HLI (Gardner, 1980). The shape and size of the xenoliths range from centimetre-size lenses, through centimetre-thick flakes up to ~1 m long rafts aligned parallel to the mineral lamination, to large blocks up to several metres thick and tens of metres long with preserved folded lithological banding (Fig. 5). Centimetre-sized xenolithic lenses are abundant in the BZ but their amount decreases away from the intrusive contact. Xenolithic material is rare in the LZ. Thin xenolith flakes are abundant in the MZ, although the xenoliths never make up more than ~5% of the rock volume, whereas the larger blocks occur only in the uppermost portion of MZb and the UZ. In the UZ the xenoliths locally make up 40% of the rock volume. The recrystallized xenoliths are mainly composed of quartz, orthopyroxene and plagioclase, and often consist of alternating bands of bluish quartzite, variably feldspathic and quartz-bearing pyroxenite, norite and anorthosite reflecting high-temperature reconstitution during partial melting and diffusional exchange with the enclosing basic magma (Gardner, 1980).

SAMPLING AND ANALYSIS

Modal layering in the Hasvik cumulates is subdued and the cumulates commonly have near-eutectic modal proportions, so the collection of representative samples presents few problems. This study is based on 40 new, 3–5 kg samples taken while carefully avoiding weathered surfaces, hydrothermal veins and strongly recrystallized rocks. Samples of cumulates and country rocks are from a profile through near-continuous coastal exposures, with additional samples of representative country rock (CT4) and chilled mafic rocks (P337 and CT5) from the western contact of the intrusion (Fig. 3). P337 was collected earlier by P. Gardner, and its exact location is not known to the present authors.

Plagioclase, orthopyroxene, augite and olivine compositions were determined with a JEOL JXA-8600 electron microprobe at the University of Aarhus, using a combination of wavelength dispersive (WDS) and energy dispersive (EDS) methods. Analyses were carried out using a 20 kV acceleration voltage, 10 nA beam current and a ~2 mm beam width, using synthetic and natural standards for element calibration and ZAF correction procedures. For pyroxene Mg, Al, Si, Ca and Fe were measured by EDS with a 250 s counting time, and Na, Ti, Cr and Mn by WDS, using a 40 s counting time. For olivine EDS (120 s) was used for Mg, Si and Fe, and WDS for Ni and Mn (40 s). Finally, for plagioclase EDS (200 s) was used for Na, Al, Si and Ca, and WDS (40 s) for K and Fe. Mineral compositions were commonly characterized by a total of 6–9 spot analyses from the cores of at least three cumulus crystals within each sample.

Samples for whole-rock analysis of major and trace elements, and Sr–Nd isotopes, were prepared using a steel jaw crusher and an agate mortar at the University of Bergen (UiB). Major-element compositions were determined by X-ray fluorescence (XRF), using an automated Philips PW1404 spectrometer at UiB. SiO_2, TiO_2, Fe_2O_3, MnO, MgO, CaO, Na_2O, K_2O and P_2O_5 were analysed using glass beads prepared as described by Padfield & Gray (1971). FeO was determined by titration with potassium dichromate. The relative standard deviation (100% × 1 s/concentration) was below 2% for all measured oxides, apart from P_2O_5 (3·2%), for 20 repeat analyses of an internal gabbro standard (M. Tysseland, personal communication, 1996). Concentrations of V, Cr, Ni, Cu, Zn, Y, Zr, Nb, Ba and Ce were determined by XRF on pressed powder pellets (UiB). Relative standard deviations for 20 repeat analyses were typically below 3%, with the exception of Nb, Ba and Ce where they were up to 24%.

Isotopic analysis were performed at Mineralogical–Geological Museum, Oslo, following procedures described by Andersen (1997). Separates of Rb, Sr, Sm and Nd for isotopic analysis were prepared from homogenized powders by standard ion-exchange procedures. A fully automated Finnegan MAT262 mass-spectrometer was used to determine the isotopic ratios of Sr and Nd. Concentrations of Rb, Sr, Sm and Nd were determined by isotope dilution on spiked aliquots, using a VG354 mass spectrometer. Repeat analyses of the Johnson and Matthey Nd standard (batch S819093A) during the period of analyses yielded an average of $^{143}Nd/^{144}Nd = 0{\cdot}511101 \pm 0{\cdot}000013$ (2σ) ($n = 32$), consistent with a recommended value of 0·511107. An average of $^{87}Sr/^{86}Sr = 0{\cdot}710228 \pm 0{\cdot}000050$ (2σ) ($n = 38$) for the NBS987 Sr standard is consistent with a recommended value of 0·710245. The data reported in Table 1 have not been adjusted to these values. Some samples (CT5 and P337 for Rb, Sr, Sm and Nd; and CT29, 33, 35 and 45 for Sm and Nd) were analysed with a Finnegan 262 mass spectrometer at the UiB, following procedures similar to those described above (Pedersen *et al.*, 1996).

RESULTS

The new compositional data are summarized in Table 1. The complete datasets with mineral, whole-rock major-element, trace-element and Sr–Nd isotope compositions can be downloaded from the *Journal of Petrology* web site at http://www.oup.co.uk/petroj/hdb/Volume_40/Issue_03/dataset or can be obtained from the senior author.

Stratigraphic systematics of the Layered Series

Figures 6 and 7 show the variation in mineral compositions, whole-rock *mg*-number, Sr and Nd concentrations, and initial $^{87}Sr/^{86}Sr$ and ε_{Nd} with stratigraphic position (H). The *mg*-number [$Mg/(Mg + Fe^{2+})$] of whole-rock samples first increases smoothly up-section in the BZ and lowermost LZ from 0·655 to a high of 0·746 at the 163 m level, then remains fairly constant in the remaining LZ (0·720–0·731), and finally displays a steady decrease through the MZa to 0·661 at 789 m (Fig. 6); the *mg*-number in these rocks reflects the bulk composition of the mafic silicate minerals. The appearance of Fe–Ti oxides at the base of the MZb offsets the *mg*-number trend to lower values (0·520), but the up-section decreasing trend is maintained into the UZ, reaching a value of 0·303 at 1447 m. Two samples, at respectively 1066 and 1125 m, deviate from the decreasing *mg*-number trend because of a higher proportion of mafic silicates relative to eutectic mineral proportions.

The X_{An} [Ca/(Ca + Na)] of plagioclase increases from 0·62 to 0·71 up-section through the BZ and the lower half of the LZ (0–249 m) (Fig. 6). Within the upper half of the LZ (249–377 m), in contrast, X_{An} jumps between

Table 1: Summary of compositional data,[1] Hasvik Layered Intrusion, Norway

Sample no.	Zone	Height (m)	*mg*-no.[2] Whole rock	X_{An} (1σ)[3] Plag.	*mg*-no. (1σ)[4] Opx	*mg*-no. (1σ)[4] Augite	X_{Fo} (1σ)[4] Olivine	Sr[5] (ppm)	$^{87}Rb/^{86}Sr$	$^{87}Sr/^{86}Sr$ (2σ)[6] (700 Ma)	Nd[5] (ppm)	$^{147}Sm/^{144}Nd$	$^{143}Nd/^{144}Nd$[7] (700 Ma)	ε_{Nd} (2σ)[7] (700 Ma)
Mafic cumulate														
CT44	UBS	1568	0·443	0·529 (36)	0·566 (12)	0·693 (15)		652·5	0·044	0·705375 (34)	10·03	0·207	0·511546	−3·69 (12)
CT43	UBS	1551	0·450					518·3	0·047	0·705183 (80)	10·75	0·251	0·511344	−7·63 (39)
CT41	UZ	1447	0·303	0·530 (26)	0·398 (6)			533·7	0·027	0·708906 (28)	29·22	0·174	0·511569	−3·24 (68)
CT40	UZ	1397	0·362	0·517 (12)	0·473 (8)			514·0	0·004	0·708653 (39)	27·70	0·144	0·511748	0·26 (14)
CT35	MZb	1273	0·480	0·548 (16)	0·639 (9)	0·751 (8)		461·2	0·011	0·707125 (24)	3·60	0·170	0·511835	1·95 (14)
CT34	MZb	1226	0·490											
CT33	MZb	1181	0·494	0·581 (6)	0·663 (9)	0·753 (16)		494·3	0·010	0·706759 (16)	3·30	0·171	0·511806	1·39 (12)
CT32	MZb	1125	0·596											
CT31	MZb	1066	0·566	0·571 (12)	0·661 (10)	0·775 (17)		512·5	0·005	0·706543 (16)	3·10	0·207	0·511714	−0·41 (14)
CT30	MZb	1013	0·507	0·580 (8)	0·693 (10)	0·773 (8)								
CT29	MZb	959	0·501	0·582 (10)	0·702 (13)	0·787 (7)		459·9	0·008	0·706132 (14)	2·90	0·177	0·511836	1·97 (16)
CT28	MZb	907	0·504											
CT27	MZb	843	0·520	0·575 (25)	0·716 (7)	0·785 (—)		400·5	0·019	0·705799 (22)	2·86	0·185	0·511810	1·46 (16)
CT26	MZa	789	0·661	0·618 (29)	0·713 (10)									
CT25	MZa	747	0·662	0·604 (9)				521·1	0·019	0·705171 (26)	2·89	0·164	0·511830	1·86 (16)
CT24	MZa	692	0·679											
CT23	MZa	648	0·679	0·601 (15)	0·728 (6)	0·798 (18)		522·8	0·018	0·704670 (40)	3·30	0·147	0·511878	2·80 (16)
CT22	MZa	600	0·688	0·614 (18)	0·736 (7)	0·802 (6)								
CT21	MZa	564	0·699	0·611 (8)	0·739 (4)	0·796 (2)		511·6	0·013	0·704732 (20)	3·32	0·144	0·511868	2·60 (10)
CT20	MZa	530	0·695	0·625 (6)	0·748 (4)	0·807 (6)								
CT19	MZa	505	0·717	0·611 (17)	0·740 (13)	0·816 (2)		458·7	0·070	0·704432 (18)	4·67	0·161	0·511979	4·76 (51)
CT18	MZa	444	0·714	0·615 (7)	0·759 (3)	0·820 (10)		342·6	0·016	0·704531 (16)	3·98	0·184	0·511867	2·57 (14)

Table 1: continued

Sample no.	Zone	*Height* (m)	*mg*-no.[2] Whole rock	X_{An} (1σ)[3] Plag.	*mg*-no. (1σ)[4] Opx	*mg*-no. (1σ)[4] Augite	X_{Fo} (1σ)[4] Olivine	Sr[5] (ppm)	$^{87}Rb/^{86}Sr$	$^{87}Sr/^{86}Sr$ (2σ)[6] (700 Ma)	Nd[5] (ppm)	$^{147}Sm/^{144}Nd$	$^{143}Nd/^{144}Nd$[7] (700 Ma)	ε_{Nd} (2σ)[78] (700 Ma)
CT17	LZ	377	0·720	0·642 (30)		0·828 (8)	0·782 (5)	469·2	0·020	0·703836 (20)	4·76	0·165	0·511946	4·12 (20)
CT16	LZ	335	0·728	0·718 (8)	0·762 (10)	0·806 (16)	0·761 (2)	517·7	0·011	0·703796 (14)	3·87	0·160	0·511953	4·26 (23)
CT15	LZ	297	0·731	0·662 (20)	0·769 (6)	0·802 (10)		301·0	0·005	0·704354 (20)	4·86	0·191	0·511872	2·68 (31)
CT14	LZ	249	0·726	0·706 (18)		0·825 (7)	0·750 (4)	374·3	0·028	0·704198 (16)	4·05	0·185	0·511884	2·91 (14)
CT13	LZ	209	0·723	0·680 (8)	0·768 (3)	0·819 (7)	0·749 (2)	419·0	0·016	0·704425 (18)	4·10	0·178	0·511879	2·81 (18)
CT12	LZ	163	0·746	0·671 (45)		0·844 (10)	0·771 (3)	315·1	0·014	0·704294 (18)	2·87	0·176	0·511911	3·45 (16)
CT11	LZ	117	0·727					161·6	0·062	0·703932 (24)	4·13	0·173	0·511897	3·17 (16)
CT10	LZ	107	0·715	0·640 (15)	0·745 (5)	0·806 (6)								
CT9	LZ	82	0·688	0·628 (14)	0·712 (10)	0·817 (9)		452·7	0·037	0·704761 (16)	3·71	0·160	0·511828	1·82 (12)
CT8	BZ	65	0·699	0·662 (36)	0·713 (24)									
CT7	BZ	50	0·677	0·620 (14)	0·708 (25)	0·809 (11)		430·9	0·025	0·704702 (48)	3·91	0·168	0·511840	2·06 (16)
CT6	BZ	22	0·655											
Mafic chill														
CT5	MBS	—	0·591					448·1	0·086	0·704481 (15)	10·20	0·148	0·511890	3·03 (8)
P337"	MBS	—	0·680					173·5	0·063	0·703897 (13)	8·60	0·156	0·511881	2·85 (12)
Country rock														
CT1	Aureole	5*	0·471					562·9	0·017	0·708421 (20)	9·22	0·100	0·511564	−3·34 (25)
CT2	Aureole	50*	0·346					368·3	0·098	0·719837 (24)	30·89	0·096	0·511460	−5·37 (27)
CT3	Aureole	100*	0·305					251·3	2·557	0·715885 (18)	80·41	0·114	0·511431	−5·94 (14)
CT4	Aureole	45*	—					111·4	1·428	0·718041 (18)	15·51	0·102	0·511408	−6·39 (14)

[1]The complete dataset is available electronically at the *Journal of Petrology* web site, or from the senior author.
[2]*mg*-number = $Mg/(Mg + Fe^{2+(tot)})$ using cation fractions.
[3]$X_{An} = Ca/(Ca + Na)$ is calculated using cation fractions. Reported values are the arithmetic average with 1σ of last significant digits in parenthesis.
[4]*mg*-number and X_{Fo} calculated as $Mg/(Mg + Fe^{2+(tot)})$ using cation fractions. Reported values are the arithmetic average with 1σ of last significant digits in parenthesis.
[5]Determined by isotope dilution.
[6]Sr calculations assumes the decay constant $\lambda^{87}Rb = 1{\cdot}42e^{-11}$/year. Values for $^{87}Sr/^{86}Sr$ are normalized to $^{86}Sr/^{88}Sr = 0{\cdot}1196$.
[7]Nd calculations assume the decay constant $\lambda^{147}Sm = 6{\cdot}54e^{-12}$/year and CHUR (700 Ma) $^{143}Nd/^{144}Nd = 0{\cdot}51173$. Values for $^{143}Nd/^{144}Nd$ are normalized to $^{146}Nd/^{144}Nd = 0{\cdot}721903$. Uncertainties for ε values σ are propagated analytical values (in parentheses).
*Distance from intrusive contact (m).

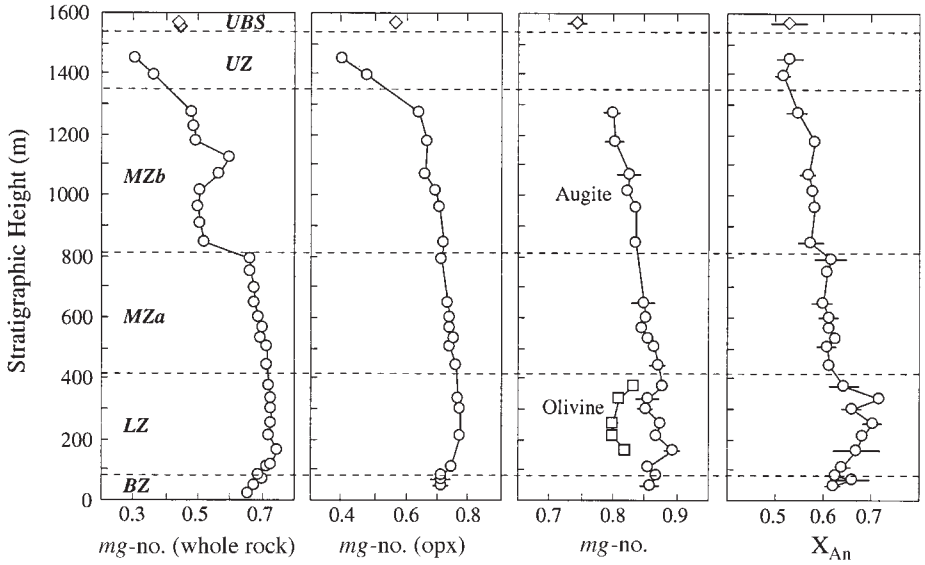

Fig. 6. Compositional variation of *mg*-number (whole rock), orthopyroxene (*mg*-number), augite (*mg*-number), olivine (*mg*-number = X_{Fo}) and plagioclase (X_{An}) with stratigraphic position in the studied section. BZ, LZ, MZ and UZ refer to sub-zones as defined in Fig. 4. UBS, Upper Border Series. Mineral analyses represent the average of 5–9 core compositions in each sample; horizontal bars give 1 SD ($\pm 1\sigma$) when this value exceeds the size of the symbol.

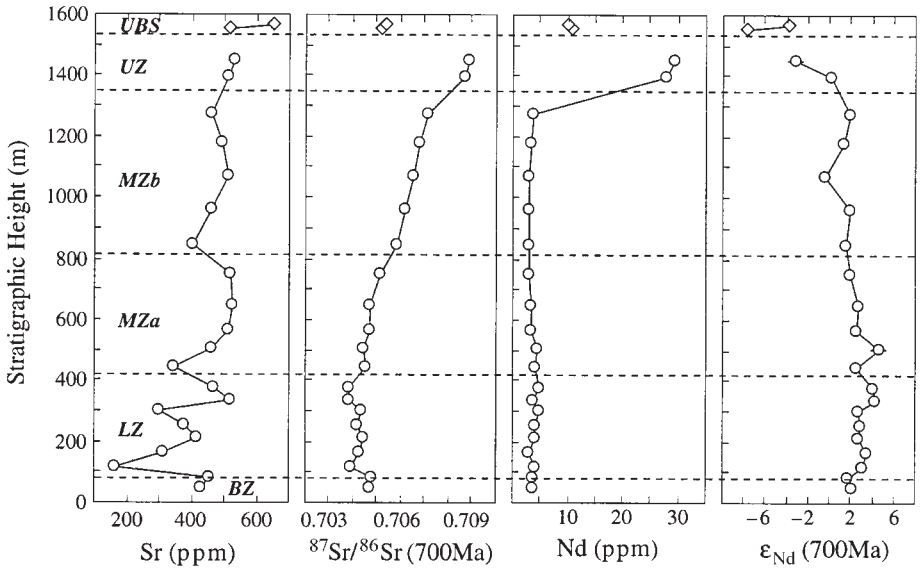

Fig. 7. Compositional variation of $^{87}Sr/^{86}Sr$ and ε_{Nd}, corrected for the decay of ^{87}Rb and ^{147}Sm to 700 Ma, plotted against stratigraphic position together with the concentration of Sr and Nd. Horizontal bars that represent the analytical uncertainty (2σ) on $^{87}Sr/^{86}Sr$ and ε_{Nd} only rarely exceed the size of symbols used.

0·72 and 0·64. Across the LZ–MZ boundary X_{An} drops to 0·62 (444 m) then fairly steadily decreases to 0·52 near the top of the UZ. The *mg*-number of the mafic minerals generally mimics that for whole rocks and the compositional trend for plagioclase (Fig. 6), suggesting mineralogical equilibrium. The *mg*-number of orthopyroxene increases from 0·71 to 0·77 from the base of the BZ to the middle of the LZ (0–297 m); this is followed first by a steady decrease to 0·64 at the top of the MZ (1273 m), and finally a rapid decrease to 0·39 in the UZ. The *mg*-number of augite varies erratically (0·81–0·84) in the BZ and LZ before showing a steadily decreasing trend reaching 0·75 in the upper part of the MZ, where cumulus augite disappears. Olivine compositions in the

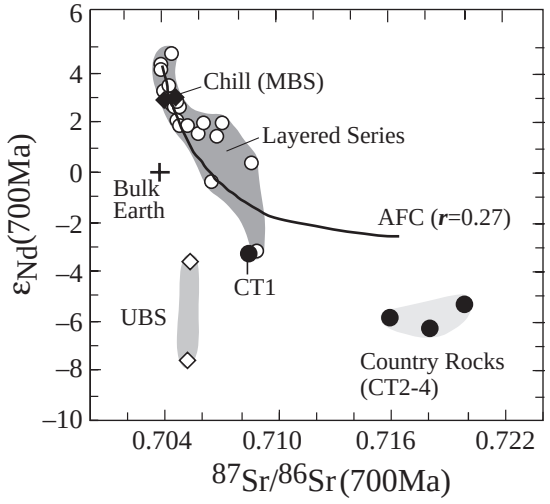

Fig. 8. Variations in ε_{Nd} and $^{87}Sr/^{86}Sr$ among the cumulates of the Layered Series, the Upper Border Series (UBS: CT43 and CT44), the chilled mafic rocks of the Marginal Border Series (MBS: P337 and CT5), and crustal country rocks (CT1–4). Also shown is the isotopic composition of Bulk Earth. The continuous curve shows the calculated evolution of Sr and Nd isotopes during coupled assimilation and fractional crystallization (AFC) for r set to 0·27. The AFC modelling is based on equations (1) and (2) explained in the text and input parameters summarized in Table 3.

LZ vary in a tight range (0·75–0·78) but correlate approximately with augite and show the most primitive compositions at the base and top of this zone.

Initial $^{87}Sr/^{86}Sr$ generally decreases from ~0·7047 to 0·7038 up-section through the BZ and most of LZ (0–335 m) (Fig. 7). Sample CT11 (117 m), which deviates slightly from this decreasing trend, may possibly be explained by post-crystallization alteration causing overcorrection for Rb decay as suggested by its unusually high $^{87}Rb/^{86}Sr$ ratio (0·0619) (Table 1). Initial ε_{Nd} increases from +1·87 to +4·26 for the same stratigraphic interval and correlates inversely with $^{87}Sr/^{86}Sr_i$. Above 335 m, $^{87}Sr/^{86}Sr$ increases remarkably smoothly from ~0·7038 to ~0·7089 at 1447 m within the upper portion of the UZ and displays a strong negative correlation with mineral compositions. ε_{Nd} shows a more erratic but generally decreasing trend up-section in the MZ from +4·26 at 335 m to +1·95 at 1273 m, followed by a rapid decrease to –3·24 in the UZ (1447 m). Sample CT31 (1066 m) deviates significantly from the general stratigraphic trend of ε_{Nd} and has a higher $^{147}Sm/^{144}Nd$ than adjacent samples (Table 1), implying a relatively large age correction on $^{143}Nd/^{144}Nd$. This may possibly be the result of metamorphic disturbance, although the more easily disturbed Rb–Sr system is not affected. ε_{Nd} exhibits an imperfect positive correlation with mineral compositions, in particular *mg*-number of orthopyroxene, and a crude negative correlation with $^{87}Sr/^{86}Sr$ (Fig. 8).

Upper Border Series

The composition of two apatite–oxide gabbro–norite samples from the Upper Border Series differs from any particular stratigraphic level of the floor cumulates represented by the Layered Series. The whole-rock *mg*-number (0·44–0·45), orthopyroxene *mg*-number (0·57) and X_{An} (0·53) for the Upper Border Series correspond approximately to values at the MZb–UZ boundary (Fig. 6). Conversely, the $^{87}Sr/^{86}Sr$ values (0·7052–0·7054) for the Upper Border Series correspond more closely to values at the MZa–MZb boundary (Fig. 7). The ε_{Nd} values for the Upper Border Series (–3·7 to –7·6) are the lowest measured within the igneous rocks of the HLI, and compare with values for the adjacent country rocks (–5·4 to –6·4) (Fig. 8).

Marginal Border Series

Two samples of sub-ophitic olivine microgabbro from the Marginal Border Series, P337 with 11% hypersthene and 8% olivine and CT5 with 21% hypersthene and 1% quartz in the CIPW norm, have tholeiitic compositions that are consistent with the Hasvik differentiation sequence, and are strikingly similar to parental magma estimates for the Skaergaard intrusion (Table 2). Judged from the major element composition, e.g. SiO_2 (49·61 wt %), TiO_2 (1·79 wt %) and MgO (7·63 wt %) contents, sample CT5 is comparable with common basalts and may represent a true chill that is virtually unmodified by crystal accumulation. The calculated X_{Fo} of olivine in equilibrium with CT5, using $K_D^{olivine\text{-}liquid} = 0{\cdot}30$ (Roeder & Emslie, 1970), is 0·83. This value is ~5 mol % higher than the most magnesian olivine of the Layered Series ($X_{Fo} = 0{\cdot}78$), but, considering the effect of equilibration with trapped liquid to lower X_{Fo} values in cumulate rocks (Barnes, 1986), a magma with the composition of CT5 is entirely consistent with the most primitive cumulates of the HLI. The low *mg*-number (0·591) and low Ni content (35 ppm) of CT5 relative to primary mantle melts, and the scarcity of ultramafic cumulates in the HLI, suggests that the parental magma to the studied section had already undergone fractional crystallization. Sample P337, which has higher *mg*-number (0·68) and Ni (552 ppm) content, and lower Y, Zr, Nb, Ce and Nd contents than CT5 (Table 2), is considered to be slightly accumulative.

Sr and Nd isotopic compositions of CT5 and P337 show that the chilled rocks have slightly lower ε_{Nd} (+3·03 and +2·85) and slightly higher $^{87}Sr/^{86}Sr$ (0·7045 and 0·7039) than the most primitive cumulates of the Layered Series. The Sr composition of the chilled rocks is slightly higher than the composition of the Bulk Silicate Earth at 700 Ma [$^{87}Sr/^{86}Sr = 0{\cdot}703685$ (UR)], suggesting some

Table 2: X-ray fluorescence analyses of chilled marginal rocks, Hasvik Layered Intrusion and Skaergaard Intrusion

Intrusion:	Hasvik	Hasvik	Skaergaard	Skaergaard
Sample no.:	CT5	P337[1]	KT-39[2]	EG4507[3]
Rock type:	chill	chill	chill	chill
Major element (wt %)				
SiO_2	49·61	49·57	49·62	48·08
TiO_2	1·79	1·02	2·61	1·17
Al_2O_3	15·01	15·55	13·25	17·22
FeO	6·69	7·15	11·48	8·44
Fe_2O_3	3·05	0·79	1·72	1·32
MnO	0·16	0·14	0·22	0·16
MgO	7·63	9·37	7·23	8·62
CaO	11·63	12·87	10·13	11·38
Na_2O	2·04	2·10	2·39	2·37
K_2O	0·37	0·27	0·45	0·25
P_2O_5	0·09	0·14	0·22	0·10
LOI	0·53	0·47	—	1·01
Sum	98·60	99·44	99·32	100·12
mg-no.[4]	0·591	0·680	0·497	0·615
Trace element (ppm)				
Cr	130	320	199	170
Ni	35	552	141	180
Y	15	7	29	—
Zr	62	39	159	50
Nb	8	4	16	—
Ba	187	110	96	40
Ce	24	14	32	—

[1]Robins & Takla (1979) and Gardner (1980).
[2]Hoover (1989).
[3]Wager & Brown (1968).
[4]*mg*-number = $Mg/(Mg + Fe^{2+(tot)})$ using molar proportions.

contamination by crustal rocks as shown below. The positive ε_{Nd} for the chilled rocks suggests a depleted mantle source.

Effects of Caledonian metamorphism

Primary igneous minerals and textures are generally well preserved in the HLI. However, regional metamorphism has locally resulted in recrystallization of the cumulates, including the development of two pyroxene–spinel coronas between olivine and plagioclase, mantling of augite by hornblende and quartz, crystallization of biotite around Fe–Ti oxides, garnet growth around biotite (where garnet is intergrown with Fe–Ti oxides) and orthopyroxene (where garnet and pyroxene are separated by a quartz rim), and replacement of orthopyroxene by anthophyllite and cummingtonite.

The effect of this metamorphism on the primary compositions is considered to be minimal for carefully selected samples. Mineral compositions as determined by electron microprobe analysis of the cores of cumulus grains do not seem to have been affected by diffusional exchange with metamorphic overgrowths. Possible changes of isotopic ratios and elemental compositions of rocks are more difficult to evaluate; the best indicator probably is the consistency of the observed data. Mineral–whole-rock Sm–Nd data from two samples of the HLI cumulates yield isochrons that are identical within error (Daly *et al.*, 1991), strongly suggesting negligible disturbance of the Sm–Nd systematics. Likewise, the secular trends for isotopic ratios and whole-rock compositions discussed below are consistent with the measured primary mineralogy, and isotopic Nd–Sr ratios similar to mantle values for chilled rocks and the most primitive cumulates strongly suggest preservation of the primary values.

DISCUSSION

A magma chamber model

Field observations, petrography, mineralogy and geochemistry constrain a complex history of magma chamber processes in the HLI and necessitate revision of earlier models (Robins & Gardner, 1974; Gardner, 1980; Robins, 1985). A magma chamber model is proposed which includes crystallization from a stratified magma column with four principal layers.

The basal ~335 m of cumulates (i.e. the BZ and lower portion of the LZ) record the emplacement of magma into the chamber. The up-section increase in X_{An} and *mg*-number of the mafic minerals and cumulates, together with the presence of olivine in the LZ, suggests that the parental magma became more primitive (hotter) with time (Robins & Gardner, 1974). The alternative explanations of a basal quench effect (Campbell, 1977; Raedeke & McCallum, 1984; Chalokwu & Grant, 1990), or variations in oxygen fugacity during magma emplacement (Loney & Himmelberg, 1983), cannot explain the correlation of mineral and isotopic compositions. Moreover, the up-section increase in $^{87}Sr/^{86}Sr$ and decrease in ε_{Nd} confirm that the emplaced magma became not only more primitive, but also less contaminated with time as originally proposed by Robins & Gardner (1974). This implies either a mixing relation between recharging primitive magma (hot and relatively little contaminated) and pre-existing, more evolved and contaminated magma (Gray & Goode, 1989), or, alternatively, the elevation of a stratified magma along an inward-sloping magma chamber floor during chamber expansion (Wilson & Engel-Sørensen, 1986; Sørensen & Wilson, 1995). The

large variations in plagioclase compositions (up to 7 mol % X_{An}) in the interval 249–377 m imply differences in magma temperature of ~45°C between adjacent cumulate layers (Deer *et al.*, 1992). This inference is supportive of a two-component magma-mixing hypothesis and cannot be reconciled with a model based solely on the expansion of a stratified magma chamber. We therefore surmise that the basal sequence of the HLI (0–335 m) reflects recharge by primitive, uncontaminated magma and mixing with pre-existing, more evolved magma in the chamber with an up-section increase in the ratio of new to pre-existing magma, with some irregularities caused by imperfect mixing.

The middle portion of the cumulate sequence (335–1360 m), i.e. the upper portion of the LZ and the MZ, reflects apparently uninterrupted fractional crystallization akin to the tholeiitic fractionation trend of the Skaergaard intrusion (Wager & Brown, 1968; McBirney, 1996). This inference is supported first by the up-section disappearance of cumulus olivine (olivine–melt reaction) and the subsequent appearance of cumulus orthopyroxene, Fe–Ti oxides (magnetite and ilmenite), and the reappearance of olivine (Fig. 4) and, second, by the smooth up-section decrease in X_{An} and *mg*-number of the mafic minerals and whole rocks (Fig. 6). However, in marked contrast to the Skaergaard intrusion (Stewart & DePaolo, 1990; McBirney, 1996), the smooth up-section increase in $^{87}Sr/^{86}Sr_i$ and the correlation with ε_{Nd} and mineral compositions of the HLI (Figs 1, 6 and 7) imply concurrent assimilation of crustal rocks and fractional crystallization (AFC), to be discussed in detail below.

The cumulates of the UZ (1360–1550 m) crystallized last, from a magma that was evolved relative to the parental magma to the MZ, as witnessed by the mineral compositions (Fig. 6). However, the phase transitions across the MZb–UZ boundary, i.e. the appearance of apatite and pigeonite as cumulus phases and the disappearance of olivine and augite (Fig. 4), deviate from a normal tholeiitic differentiation trend (Irvine, 1979). In particular, the disappearance of cumulus augite is unusual and has tentatively been related to the assimilation of country rocks (Robins & Gardner, 1974). This is discussed further below.

The Upper Border Series is characterized by large amphibole oikocrysts and hence crystallized from a hydrous magma that was unlike the evolving magma responsible for the Layered Series. The Upper Border Series probably represents the crystallization of a hybrid magma of partly fused country rock and basalt at the roof of the chamber (Gardner, 1980). The distinct Sr–Nd isotopic compositions of the Upper Border Series relative to the Layered Series (Fig. 8) imply that there was little or no material exchange between this magma residing beneath the roof and the remaining magma in the Hasvik chamber, as is inferred for the Vandfaldsdalen macrodyke in East Greenland (Geist & White, 1994).

Assimilation and fractional crystallization

The correlation between mineral and whole-rock compositions and Sr–Nd isotopic ratios within the Middle and Upper Zone cumulates of the HLI suggests that crustal assimilation and fractional crystallization (AFC) were concurrent processes. Below we apply conventional AFC calculations to the cumulates of the HLI, aiming to quantify the amount of crustal assimilation.

Background and formalism

The effects of crustal assimilation on the evolution of basaltic magmas were discussed early on by Bowen (1928) and Wilcox (1954). In a remarkable study of the lava suite of Parícutin, Mexico, Wilcox (1954) demonstrated that AFC can explain its calc-alkaline liquid line of descent. Both Bowen (1928) and Wilcox (1954) pointed out that the heat required to assimilate crust could be supplied by the release of latent heat of crystallization. In doing so, Wilcox and Bowen made it clear that superheated magmas were not necessary for assimilation to take place and established the basis for the modern treatment of AFC (Taylor, 1980; DePaolo, 1981, 1985; McBirney *et al.*, 1987). The formalism used here for trace-element and isotopic modelling of AFC was first developed by DePaolo (1981, 1985). The change in isotopic ratios with mass crystallized is (after Stewart & DePaolo, 1990)

$$de_m/dM_c = 1/M[rC_a/C_m(e_a - e_m)] \quad (1)$$

where C_m changes with r and D_c:

$$dC_m/dM_c = 1/M[r(C_a - C_m) - C_m(D_c - 1)]. \quad (2)$$

The variables are defined as follows: e_m is the isotopic ratio of the magma, e_a is the isotopic ratio of the assimilant, M is the mass of remaining magma in the chamber, M_c is the mass of crystallized magma, r is the ratio of the rate of assimilation to the rate of crystallization (M_a/M_c, where M_a is the mass of assimilated material), C_m is the element concentration in the magma, C_a is the element concentration in the assimilant, D_c is the effective distribution coefficient between magma and cumulates, and subscript i denotes initial values before the onset of crystallization (e.g. C_{mi} is the initial element concentration in magma).

Rigorous AFC modelling requires precise constraints on the composition of the parental magma (e_m, C_m) and the assimilated crustal material (e_a, C_a), the bulk distribution coefficients (D_c) and, finally, in the case of modelling isotopic data from cumulates, the conversion

of stratigraphic position (*H*) shown in Fig. 4 to fraction of melt remaining in the system ($F = M/M_i$).

Parental magma composition

Constraints on initial e_m and C_m are provided by the composition of chilled rocks from the Marginal Border Series and the composition of the most primitive cumulates in the Layered Series. We concluded earlier that CT5 can reasonably represent the parental magma composition and hence we use $C_{mi} = 10{\cdot}2$ ppm for Nd and 448·1 ppm for Sr in the modelling of AFC. Sr and Nd isotopic compositions of CT5 and P337 are plotted in Fig. 8 together with cumulates from the Layered Series and country rocks. The chilled rocks have slightly lower ε_{Nd} (+3·03 and +2·85) and slightly higher $^{87}Sr/^{86}Sr$ (0·7045 and 0·7039) than the most primitive cumulates of the Layered Series with $\varepsilon_{Ndi} = +4{\cdot}76$ (CT19) and $^{87}Sr/^{86}Sr = 0{\cdot}7038$ (CT16), but still plot within the least contaminated end of the isotopic array defined by the Layered Series. This is suggestive of slight contamination with the adjacent wall rocks against which the Marginal Border Series crystallized. For the purpose of AFC modelling the most primitive cumulates of the Layered Series are considered the more realistic constraints for e_{mi}. Sample CT16 collected at 335 m in the LZ, which has the least radiogenic $^{87}Sr/^{86}Sr$ (0·7038), the second highest ε_{Nd} (+4·26), and the most calcic plagioclases ($X_{An} = 0{\cdot}72$) in the Layered Series, is chosen to represent the isotopic composition of the parental magma.

Bulk distribution coefficients

The variation of Sr concentrations in the MZ and UZ cumulates is limited (343–534) and not particularly systematic with respect to stratigraphic height (Fig. 7), suggesting an effective bulk distribution coefficient (D_c) close to unity. This is in agreement with a $D_c(Sr) = 0{\cdot}95$ calculated using average mineral–melt *D* values (Henderson, 1982), a realistic modal composition for the cumulates, and assuming 10% trapped liquid. This is the D_c that has been assumed in AFC calculations.

Nd concentrations are low and fairly constant (2·9–4·9 ppm) in cumulates of the LZ and MZ, but reach much higher values (28–29 ppm) in the UZ because of abundant cumulus apatite (Fig. 7). For the purpose of AFC modelling a constant $D_c(Nd) = 0{\cdot}29$ has been assumed, calculated as outlined above for Sr. This value is consistent with the Nd content in the chilled rocks; cumulates that crystallized from CT5 (10·2 ppm Nd) would have ~3·0 ppm Nd.

Composition of crustal assimilants

The composition of likely assimilants is crucial to AFC modelling. Constraints on e_a and C_a come traditionally from the bulk composition of the adjacent country rocks (Wilcox, 1954; DePaolo, 1985; Grunder, 1987; McBirney *et al.*, 1987; Stewart & DePaolo, 1990; Nielsen *et al.*, 1996; Reiners *et al.*, 1996), partial melts of the country rocks (Wilson *et al.*, 1987; Blichert-Toft *et al.*, 1992; Sørensen & Wilson, 1995), or roof granophyres (Stewart & DePaolo, 1992, 1996).

The composition of the assimilated material in the HLI is constrained by four samples (CT1–4) from the contact metamorphic aureole at locations shown in Fig. 3. Their compositions (Table 1) reflect initial lithological variations modified to different degrees by the extraction of partial melts and equilibration with the intrusive magma. Sample CT1, collected only ~5 m from the intrusive contact, has a much more mafic composition (e.g. $SiO_2 = 47{\cdot}04$ wt % and MgO = 3·97 wt %) than samples taken further away from the intrusive contact (>60 wt % SiO_2, and MgO <1·63 wt %), suggesting reaction with the intrusive magma. Likewise, isotopic ratios in CT1 are far removed from those of the other country rocks (Table 1 and Fig. 8) and comparable only with the most contaminated cumulate sample, supporting isotopic equilibration with the intrusive magma. We conclude that the composition of sample CT1 is highly modified, and unlikely to represent the original composition of the country rocks. Similarly, most of the xenoliths within the HLI are considered to have equilibrated extensively with the surrounding magma (Gardner, 1980).

The remaining three country-rock samples are silica rich (61–88 wt % SiO_2) and show variable compositions reflecting their different lithologies (see complete dataset). The average Sr (323·4 ppm) and Nd (34·0 ppm) contents of the four samples are considered the best estimate of the bulk composition of the assimilant. Sr and Nd isotopic compositions for the country-rock samples (omitting CT1) cluster in the lower right corner of Fig. 8, suggesting an average value of $^{87}Sr/^{86}Sr = 0{\cdot}7182$ and $\varepsilon_{Nd} = -5{\cdot}86$ for e_a. These values are consistent with Sr–Nd systematics of the Sørøy Succession ~20 km to the WNW of the HLI (Aitcheson, 1989).

Conversion of stratigraphic height (H) *to fraction of magma remaining* (F)

The isotopic ratios calculated using equation (1) change with the fraction of magma remaining in the chamber (*F*). To display the results of AFC modelling against stratigraphic position (*H*) in the Layered Series, a relationship between *F* and *H* has to be derived. The approach adopted here assumes a linear relation, and an estimate of the value of *F* for the top of the studied section (F_{final}). If $F = 1$ at 335 m, the starting point of AFC calculations, the relation is

$$H = 335 + 1205F/F_{final}. \quad (3)$$

The presence of accessory apatite, interstitial quartz and

Table 3: Parameters used in AFC modelling

	Sr	Nd
Concentration in parent magma (C_m; ppm)	448·1	10·2
Initial isotopic ratio in parent magma (e_m)	*0·7038*	*+4·26*
Average concentration in country rocks (C_a; ppm)	323·4	34·0
Average initial isotopic ratio in country rocks (e_a)	*0·7182*	*−5·86*
Effective bulk partitioning coefficient (D_e)[1]	0·95	0·29

[1]Calculated assuming: 45% plagioclase, 23% orthopyroxene, 23% augite and 10% trapped liquid in the cumulates; partition coefficients (plagioclase:orthopyroxene:augite) of 1·80:0·0:0·14 for Sr and 0·08:0·10:0·60 for Nd.

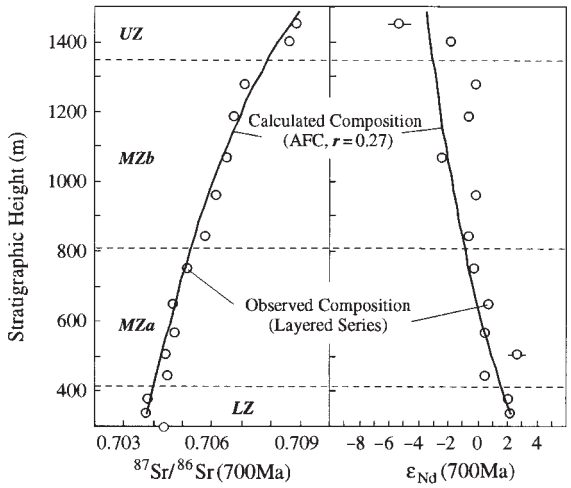

Fig. 9. Comparison of observed ε_{Nd} and $^{87}Sr/^{86}Sr$ data for cumulates of the Layered Series between 335 and 1550 m stratigraphic height judged to reflect a simple fractionation sequence and the results of AFC modelling. (See text for explanation.)

quartz–K-feldspar intergrowth in the UZ is comparable with evolved mafic cumulates in closed-system tholeiitic intrusions such as Skaergaard, Bushveld, Basistoppen and Fongen–Hyllingen (Wager & Brown, 1968; Naslund, 1989; Eales & Cawthorn, 1996; Wilson & Sørensen, 1996). However, the UZ lacks the extremely iron-rich mafic minerals and sodium-rich varieties of plagioclase found in these intrusions, implying that some fraction of the initial magma still remained in the chamber when the UZ had crystallized. We anticipate that the floor and roof cumulates of the exposed section met while magma was still present in a more central portion of the HLI (now submerged; see Fig. 2), similar to the eastern part of the Skaergaard intrusion, where the Sandwich Horizon is lacking (McBirney, 1996), or, alternatively, that the remaining magma fraction was tapped.

In the above-mentioned tholeiitic intrusions the first appearance of cumulus apatite occurred when 32–21 vol. % magma remained in the chamber relative to the last major replenishment event. Using this range as an analogue for the HLI, noting that increasing P_2O_5 content of the magma primarily reflects fractional crystallization rather than assimilation of country rocks, and allowing for the crystallization of ~190 m UZ cumulates after the first appearance of apatite, suggests that F_{final} was of the order of 0·1–0·2 at the top of the exposed section. This range of F seems intuitively reasonable; in the following we therefore assume $F_{final} = 0{\cdot}15$.

Amount of assimilation

Using equations (1) and (2) and the constraints for e_{mi}, C_{mi}, D_e, e_a, C_a and F summarized in Table 3, the amount of assimilation in the cumulates above 335 m in the Layered Series can be evaluated. The approach adopted here uses equation (3) to convert resulting F to stratigraphic position (H), followed by fitting of calculated e_m(Sr) to the observed $^{87}Sr/^{86}Sr$ by varying r, the rate of assimilation to the rate of crystallization. This approach demonstrates that AFC with a constant r value of 0·27 closely reproduces the smooth up-section variations in $^{87}Sr/^{86}Sr$ of the cumulates between 335 and 1550 m (Fig. 9). Therefore, if assimilation was governed by bulk ingestion, the studied section (335–1550 m), in bulk, is made up of ~79% uncontaminated basalt and ~21% crust.

The measured Nd isotopic ratios are dispersed about the stratigraphic e_m(Nd) trend modelled by AFC for r set to 0·27 (Fig. 9). Moreover, it appears that the measured ε_{Nd} values generally lie to the right (up to 2·7 ε units) of the calculated ratios between ~800 and ~1400 m, implying a decoupling of Sr and Nd during assimilation. One possible explanation is secular changes in the composition of the assimilant, a process that is not accounted for in AFC calculations. In particular, the Nd content of the country rock is highly variable (9–80 ppm; Table 1) and up to eight times greater than the Nd content of the initial magma (10·2 ppm). Furthermore, the occurrence of granitic dykes closely associated with recrystallized xenoliths suggests that the assimilated material may have been partial melts derived from the xenoliths (Gardner, 1980). Thus, if the partition coefficient between rock and melt during partial melting is <1 for Nd and ~1 for Sr, as is expected for most xenolith compositions, progressive partial melting will result in secularly decreasing Nd content of the assimilant with time. This tendency could explain the discrepancy between modelled and measured Nd compositions in the upper portion of the Layered Series. Alternatively, the decoupling of Sr and Nd isotopes is also consistent with a xenolith–basalt reaction governed by isotopic 'self-diffusion', which is ~3 times higher for Sr than for Nd (Lesher, 1990, 1994). However, as shown

below, the crystallization sequence of the cumulates implies considerable contamination by Si and Al. These elements diffuse notably slowly (Lesher, 1990) as is witnessed by the preservation of bimodal felsic–mafic layers in many plutons (Wiebe, 1993) and distinct, buoyant granophyric roof melts in otherwise mafic magma chambers (Campbell & Turner, 1987; Stewart & DePaolo, 1992, 1996; Geist & White, 1994). We thus conclude that the Sr and Nd isotopic compositions of the HLI predominantly reflect bulk ingestion of the assimilant, perhaps with increasing Sr/Nd with time, although minor effects of selective isotopic self-diffusion may also have influenced the isotopic composition of the differentiating basaltic magma.

Role of crustal xenoliths

Bowen (1928) and Wilcox (1954) solicited the assimilation of country-rock xenoliths enclosed in magma chambers as the predominant cause of the contamination of basalt. More recent inferences from layered intrusions, however, almost unanimously suggest that the assimilated material originated from a distinct, buoyant, hybrid layer at the roof of the basaltic magma chamber (DePaolo, 1985; Campbell & Turner, 1987; Stewart & DePaolo, 1990, 1992, 1996; Sørensen & Wilson, 1995; Nielsen *et al.*, 1996). However, the study of Geist & White (1994) has demonstrated a lack of material exchange between a granophyric roof melt and the immediately underlying basaltic magma in the Vandfaldsdalen macro-dyke, East Greenland. Likewise, many of the above researchers argued that the low degree of assimilation in layered intrusions such as Skaergaard, Kiglapait and Muskox (<5% crust) is the result of restricted exchange between a granophyric roof melt and the main basaltic magma chamber (DePaolo, 1985; Stewart & DePaolo, 1990, 1992, 1996). Similarly, in the case of the HLI, the distinct isotopic compositions rule out significant material exchange between the hybrid magma from which the Upper Border Series crystallized and the parental magma to the Layered Series (Fig. 8).

In the HLI, the abundance of crustal xenoliths within the Layered Series points to a causal link between the assimilation of xenoliths and contamination of the magma. The increase in number and size of the xenoliths towards the top of the Layered Series suggests that the country-rock xenoliths spalled off the roof during lateral expansion of the chamber and remained floating in the magma with near-neutral buoyancies. If so, whole-chamber convection cannot have included the upper magma layer from which the UZ crystallized, consistent with the compositional and petrographic discontinuity between the cumulates of the MZb and the UZ. On the other hand, the highly recrystallized nature of the xenoliths found in the MZ suggests these were slightly denser than the magma (and the unmodified country-rock xenoliths) and hence were able to sink to the base of the chamber, possibly aided by convection currents. This inference is consistent with the thin, flaky appearance of the xenoliths in the MZ.

Thermal considerations

The maximum possible amount of assimilation by bulk ingestion is constrained by the total thermal budget and can be assessed by elaborating onto the equations and constants of Grunder (1995). The amount of available heat provided by a volume of magma is $[C_P(T_{basalt} - T_{final}) + L_{basalt}]$, where C_P is specific heat (~1100 J/kg per K for basalt and crust) and L_{basalt} is latent heat of crystallization ($\sim 4 \times 10^5$ J/kg). The temperature of the parental magma (T_{basalt}) is estimated to 1180°C using the MgO content of the chill sample (CT5) and experimental work on Skaergaard magmas as an analogue (Toplis & Carroll, 1995). The final temperature (T_{final}) is taken as 1025°C. The heat consumed is $[k_1 C_P(T_{aureole} - T_{initial}) + k_2 C_P(T_{final} - T_{aureole}) + L_{crust}]$; where L_{crust} is $\sim 3 \times 10^5$ J/kg; and k_1 and k_2 denote the volume (relative to the volume of partial melt) of the aureole that is heated to $T_{aureole}$ and the volume of restite xenoliths heated to T_{final}, respectively; k_2 is therefore $1/F$, where F is the melt fraction for partial melting of metapelite at T_{final} and is assumed to be 0·65 (i.e. $k_2 = 1{\cdot}54$) (Vielzeuf & Holloway, 1988). If it is then assumed that (1) the densities of crust, partial melt and basalt are the same, (2) $T_{initial}$ is 500°C and the average $T_{aureole}$ is 775°C (i.e. 100°C less than the modelled peak temperature of the contact-metamorphic mineral assemblage), and (3) k_1 is 2·6, which, in turn, corresponds to an estimated ratio of the mass of the aureole to the parental magma mass of ~0·4, then the ratio of the total mass of partial crustal melt to the total parental magma mass is ~0·38. The modelled rate, r, at which AFC occurred in the Hasvik chamber suggests that the ratio of crust to parental basalt is ~0·27, i.e. well within the amount permitted by the heat budget. In a 'worst case' with $T_{initial} = 400$°C and the average $T_{aureole} = 875$°C the resulting c_t/m_t is ~0·30 and the modelled amount of assimilation would still just be permitted by the heat budget.

The coupling of fractional crystallization and assimilation in the Hasvik magma chamber, expressed most clearly by the stratigraphic variation in mineral chemistry and $^{87}Sr/^{86}Sr$, is envisaged as being thermal. Latent heat released at the temporary floor of the magma chamber, where crystallization of the cumulates was taking place, was transported upwards through the magma column by diffusion and convection to supply the thermal energy required for local melting and assimilation. The rate r of AFC, probably ~0·27 in the Hasvik chamber, may be regarded as an expression of the efficiency of this transfer of thermal energy.

Crystallization sequence

The crystallization sequence of cumulate rocks provides a record of the compositional evolution of the magma. The cumulate sequence olivine gabbro (LZ), gabbro–norite (MZa), oxide gabbro–norite (MZb) and oxide two-pyroxene olivine gabbro (top of MZb) (Fig. 4) witnesses the progressive crystallization of a quartz-normative tholeiitic parental magma, consistent with the composition of the chilled mafic rocks (Table 2). This crystallization sequence is akin to that of the Skaergaard intrusion (Wager & Brown, 1968; McBirney, 1996). The cumulate assemblage of the UZ (plagioclase, pigeonite, oxides, apatite and rare augite), however, deviates from the most evolved cumulates of the Skaergaard intrusion, which have abundant ferroaugite and fayalite on the liquidus. We anticipate that this discrepancy reflects a fundamental difference in the liquid line of descent; in the Skaergaard intrusion closed-system fractional crystallization without concomitant crustal assimilation led to iron-rich residual magmas (Wager & Brown, 1968; McBirney, 1996) whereas, in the HLI, the large degree of crustal assimilation led to a silica-rich end-product (Robins & Gardner, 1974; Gardner, 1980). The effect of crustal assimilation on differentiated basalt has yet to be modelled experimentally. However, Bowen (1928) noted that the assimilation of silica- and aluminium-rich material into basalt would tend to stabilize Ca-poor pyroxene at the expense of Ca-rich pyroxene, resulting in a noritic differentiate. Indeed, Wilcox (1954) showed that the most primitive and least contaminated (oldest) lavas of Parícutin were saturated with plagioclase, augite, Ca-poor pyroxene and olivine, whereas the more evolved and contaminated (younger) lavas only crystallized Ca-poor pyroxene and plagioclase, but included rare relic olivine phenocrysts. This petrographic shift occurred at ~56 wt % SiO_2, perhaps a realistic value also for the SiO_2 content of the parental magma to the UZ of the HLI. More recently, the experimental work of Longhi & Pan (1988) has shown that a reaction relation exists between olivine, orthopyroxene and liquid to form pigeonite and plagioclase in differentiated basalt. If silica- and aluminium-rich material is added by the assimilation of crustal rocks, this reaction would be enhanced and involve the breakdown of augite, mainly to supply Ca to plagioclase. The latter reaction relation is consistent with the occurrence of augite cores in pigeonite grains of the Hasvik UZ.

CONCLUSIONS

The upper portion (335–1550 m) of the Layered Series of the tholeiitic Hasvik Layered Intrusion (HLI), overlying a basal zone (0–335 m) that records magma recharge and mixing, displays a remarkably smooth up-section increase in initial $^{87}Sr/^{86}Sr$ (0·7038–0·7089) that is correlative with decreasing initial ε_{Nd} (+4·76– to −3·26), *mg*-number (0·73–0·30) and mineral compositions (e.g. X_{An} = 0·72–0·52). Modelling of concurrent assimilation and fractional crystallization (AFC) on the basis of Sr and Nd isotopic compositions suggests that the ratio, *r*, of the rate of assimilation to the rate of crystallization is constant at ~0·27. Thus, in bulk, the Layered Series is composed of ~79% uncontaminated basalt and ~21% crust, placing the HLI among the most contaminated layered intrusions known. Thousands of recrystallized xenoliths of metasedimentary origin enclosed in the cumulates are thought to be the remnants of the material assimilated. The many xenoliths, which probably spalled off the roof during magma emplacement, their tabular shape and near-neutral buoyancy together with the elevated temperatures (400–600°C) of the mid-crustal country rocks, promoted a degree of assimilation in the Hasvik magma chamber close to the limit permitted by the heat budget.

ACKNOWLEDGEMENTS

We thank Grant Cawthorn and Richard Wilson for helpful and constructive comments on an early version of the manuscript. Brian Stewart, Dominique Weis and Marjorie Wilson are thanked for very thorough and thoughtful reviews. C.T. gratefully acknowledges support from the Danish National Science Research Council, and from the Geological Survey of Norway and the Danish Lithosphere Centre, where parts of this research were performed. B.R. and H.R. gratefully acknowledge the receipt of research grants from the Norwegian Research Council.

REFERENCES

Aitcheson, S. J. (1989). Crustal evolution in the Seiland region, north Norway: a Nd–Sr–Pb isotopic study. Ph.D. Thesis, National University of Ireland, Dublin, 192pp.

Andersen, T. (1997). Radiogenic isotope systematics of the Herefoss granite, South Norway: an indicator of Sveconorwegian (Grenvillian) crustal evolution in the Baltic Shield. *Chemical Geology* **135,** 139–158.

Barnes, S. J. (1986). The effect of trapped liquid crystallization on cumulus mineral compositions in layered intrusions. *Contributions to Mineralogy and Petrology* **93,** 524–531.

Blichert-Toft, J., Lesher, C. E. & Rosing, M. T. (1992). Selectively contaminated magmas of the Tertiary East Greenland macrodyke complex. *Contributions to Mineralogy and Petrology* **110,** 154–172.

Bohlen, S. R., Wall, V. J. & Boettcher, A. L. (1983). Experimental investigations and geological applications in the system FeO–TiO_2–Al_2O_3–H_2O. *American Mineralogist* **68,** 1049–1058.

Bowen, N. L. (1928). *The Evolution of Igneous Rocks*. Princeton, NJ: Princeton University Press.

Campbell, I. H. (1977). A study of cumulate processes and macrorhythmic layering in the Jimberlana Intrusion of Western Australia. Part 1: The upper layered series. *Journal of Petrology* **18,** 183–215.

Campbell, I. H. & Turner, J. S. (1987). A laboratory investigation of assimilation at the top of a basaltic magma chamber. *Journal of Geology* **95,** 155–172.

Chalokwu, C. I. & Grant, N. K. (1990). Petrology of the Partridge River Intrusion, Duluth Complex, Minnesota: 1. Relationships between mineral compositions, density and trapped liquid abundance. *Journal of Petrology* **31,** 265–293.

Dallmeyer, R. D., Mitchell, J. G., Pharaoh, T. C., Reuter, A. & Andresen, A. (1988). K–Ar and $^{40}Ar/^{39}Ar$ whole-rock ages of slate/phyllite from allochthonous basement and cover in the tectonic windows of Finnmark, Norway: Evaluating the extent and timing of Caledonian tectonothermal activity. *Geological Survey of America* **100,** 1493–1501.

Daly, J. S., Aitcheson, S. J., Cliff, R. A., Gayer, R. A. & Rice, H. N. (1991). Geochronological evidence from discordant plutons for a late Proterozoic orogen in the Caledonides of Finnmark, northern Norway. *Journal of the Geological Society, London* **148,** 29–40.

Deer, W. A., Howie, R. A. & Zussman, J. (1992). *An Introduction to the Rock Forming Minerals*, 2nd edn. Harlow, UK: Longman.

DePaolo, D. J. (1981). Trace element and isotopic effects of combined wallrock assimilation and fractional crystallization. *Earth and Planetary Science Letters* **53,** 189–202.

DePaolo, D. J. (1985). Isotopic studies of processes in magma chambers: I. The Kiglapait intrusion, Labrador. *Journal of Petrology* **26,** 925–951.

Eales, H. V. & Cawthorn, R. G. (1996). The Bushveld Complex. In: Cawthorn, R. G. (ed.) *Layered Intrusions. Developments in Igneous Petrology 15*. Amsterdam: Elsevier, pp. 181–230.

Elvevold, S., Reginiussen, H., Krogh, E. J. & Bjørklund, F. (1994). Reworking of deep-seated gabbros and associated contact metamorphosed paragenesis in the south-eastern part of the Seiland Igneous Province. *Journal of Metamorphic Geology* **12,** 539–556.

Gardner, P. (1980). The geology and petrology of the Hasvik gabbro, Sørøy, Northern Norway. Ph.D. Thesis, University of London.

Geist, D. & White, C. (1994). Assimilation and fractionation in adjacent parts of the same magma chamber: Vandfaldsdalen macrodike, East Greenland. *Contributions to Mineralogy and Petrology* **116,** 92–107.

Gray, C. M. & Goode, A. D. T. (1989). The Kalka layered intrusion, Central Australia. A strontium isotopic history of contamination and magma dynamics. *Contributions to Mineralogy and Petrology* **103,** 35–43.

Grunder, A. L. (1987). Low $d^{18}O$ silicic volcanic rocks at the Calabozos Caldera Complex, Southern Andes. *Contributions to Mineralogy and Petrology* **95,** 71–81.

Grunder, A. L. (1995). Material and thermal roles of basalt in crustal magmatism: case study from eastern Nevada. *Geology* **23,** 952–956.

Harley, S. L. (1984*a*). An experimental study of the partitioning of Fe and Mg between garnet and orthopyroxene. *Contributions to Mineralogy and Petrology* **86,** 359–373.

Harley, S. L. (1984*b*). The solubility of alumina in orthopyroxene coexisting with garnet in $FeO–MgO–Al_2O_3–SiO_2$ and $CaO–FeO–MgO–Al_2O_3–SiO_2$. *Journal of Petrology* **25,** 665–696.

Harley, S. L. & Green, D. H. (1982). Garnet–orthopyroxene barometry for granulites and peridotites. *Nature* **300,** 697–701.

Henderson, P. (1982). *Inorganic Geochemistry*. Oxford: Pergamon.

Hoover, J. D. (1989). The chilled marginal gabbro and other contact rocks of the Skaergaard intrusion. *Journal of Petrology* **30,** 441–476.

Irvine, T. N. (1979). Rocks whose composition is determined by crystal accumulation and sorting. In: Yoder, H. S. (ed.) *The Evolution of Igneous Rocks*. Princeton: Princeton University Press, pp. 245–306.

Krill, A. G. & Zwaan, K. B. (1987). Reinterpretation of 'Finnmarkian' deformation on western Sørøy, northern Norway. *Norsk Geologisk Tidsskrift* **67,** 3–13.

Krogh, E. J. & Elvevold, S. (1990). A Precambrian age for an early gabbro–monzonitic intrusive on the Øksfjord peninsula, Seiland Igneous Province. *Norsk Geologisk Tidsskrift* **70,** 267–273.

Lesher, C. E. (1990). Decoupling of chemical and isotopic exchange during magma mixing. *Nature* **344,** 235–237.

Lesher, C. E. (1994). Kinetics of Sr and Nd exchange in silicate liquids: theory, experiments, and applications to uphill diffusion, isotopic equilibrium, and irreversible mixing of magmas. *Journal of Geophysical Research* **99,** 9585–9604.

Loney, R. A. & Himmelberg, G. R. (1983). Structure and petrology of the La Perouse gabbro intrusion, Fairweather Range, southeastern Alaska. *Journal of Petrology* **24,** 377–423.

Longhi, J. & Pan, V. (1988). A reconnaisance study of phase boundaries in low-alkali basaltic liquids. *Journal of Petrology* **29,** 115–147.

McBirney, A. R. (1996). The Skaergaard Intrusion. In: Cawthorn, R. G. (ed.) *Layered Intrusions. Developments in Igneous Petrology 15*. Amsterdam: Elsevier, pp. 147–180.

McBirney, A. R., Taylor, H. P. & Armstrong, R. L. (1987). Parícutin re-examined: a classic example of crustal assimilation in calc-alkaline magma. *Contributions to Mineralogy and Petrology* **95,** 4–20.

Naslund, H. R. (1989). Petrology of the Basistoppen sill, East Greenland: a calculated magma differentiation trend. *Journal of Petrology* **30,** 299–319.

Nielsen, F. M., Campbell, I. R., McCulloch, M. & Wilson, J. R. (1996). A strontium isotopic investigation of the Bjerkreim–Sokndal layered intrusion, southwest Norway. *Journal of Petrology* **37,** 171–193.

Padfield, T. & Gray, A. (1971). Major-element rock analysis by X-ray fluoresence—a simple fusion method. *Philips Analytical Equipment Bulletin* **FS,** 35.

Pedersen, R. B., Dunning, G. R. & Robins, B. (1989). U–Pb ages of nepheline syenite pegmatites from the Seiland Magmatic Province, N Norway. In: Gayer, R. A. (ed.) *The Caledonide Geology of Scandinavia*. London: Graham & Trotman, pp. 3–8.

Pedersen, R. B., Malpas, J. & Falloon, T. (1996). Petrology and geochemistry of gabbroic and related rocks from Site 894, Hess Deep. In: Mével, C., Gillis, K. M., Allen, J. F. & Meyer, P. S. (eds.) *Proceedings of the Ocean Drilling Program, Scientific Results No. 147*. College Station, TX: Ocean Drilling Program, pp. 3–14.

Raedeke, L. D. & McCallum, I. S. (1984). Investigations in the Stillwater Complex: Part II. Petrology and petrogenesis of the ultramafic series. *Journal of Petrology* **25,** 395–420.

Reginiussen, H., Ravna, E. J. K. & Berglund, K. (1995). Mafic dykes from Øksfjord, Seiland Igneous Province, northern Norway: geochemistry and paleotectonic significance. *Geological Magazine* **132,** 667–681.

Reiners, P. W., Nelson, B. K. & Nelson, S. W. (1996). Evidence for multiple mechanisms of crustal contamination of magma from compositionally zoned plutons and associated ultramafic intrusions of the Alaska Range. *Journal of Petrology* **37,** 261–292.

Roberts, D. (1974). Hammerfest. Beskrivelse til det 1:250.000 berggrundsgeologiske kart. *Norsk Geologisk Tidsskrift* **301,** 1–66.

Robins, B. (1985). Disseminated FeTi oxides in the Seiland magmatic province of northern Norway. *Norges Geologiske Undersøkelse Bulletin* **402,** 79–92.

Robins, B. & Gardner, P. (1974). Synorogenic layered basic intrusions in the Seiland petrographic province, Finnmark. *Norges Geologiske Undersøkelse Bulletin* **312,** 91–130.

Robins, B. & Gardner, P. (1975). The magmatic evolution of the Seiland province, and Caledonian plate boundaries in Northern Norway. *Earth and Planetary Science Letters* **26,** 167–178.

Robins, B. & Takla, M. A. (1979). Geology and geochemistry of a metamorphosed picrite–ankaramite dyke suite from the Seiland province, northern Norway. *Norsk Geologisk Tidsskrift* **59,** 67–95.

Roeder, P. L. & Emslie, R. F. (1970). Olivine–liquid equilibrium. *Contributions to Mineralogy and Petrology* **29,** 275–289.

Sørensen, H. S. & Wilson, J. R. (1995). A strontium and neodymium isotopic investigation of the Fongen–Hyllingen layered intrusion, Norway. *Journal of Petrology* **36,** 161–187.

Stewart, B. W. & DePaolo, D. J. (1990). Isotopic studies of processes in mafic magma chambers: II. The Skaergaard Intrusion, East Greenland. *Contributions to Mineralogy and Petrology* **104,** 125–141.

Stewart, B. W. & DePaolo, D. J. (1992). Diffusive isotopic contamination of mafic magma chambers by coexisting silicic liquid in the Muskox Intrusion. *Science* **255,** 708–711.

Stewart, B. W. & DePaolo, D. J. (1996). Isotopic studies of processes in mafic magma chambers: III. The Muskox Intrusion, Northwest Territories, Canada. In: Basu, A. & Hart, S. (eds) *Reading the Isotopic Code. Geophysical Monograph, American Geophysical Union* **95,** 277–292.

Sturt, B. A. (1969). Wrench fault deformation and annealing recrystallization during almandine amphibolite facies regional metamorphism. *Journal of Geology* **77,** 319–332.

Taylor, H. P. (1980). The effects of assimilation of country rocks by magmas on $^{18}O/^{16}O$ and $^{87}Sr/^{86}Sr$ systematics in igneous rocks. *Earth and Planetary Science Letters* **47,** 243–254.

Toplis, M. J. & Carroll, M. R. (1995). An experimental study of the influence of oxygen fugacity on Fe–Ti oxide stability, phase relations, and mineral–melt equilibria in ferro-basaltic systems. *Journal of Petrology* **36,** 1137–1170.

Vielzeuf, D. & Holloway, J. R. (1988). Experimental determination of the fluid-absent melting relations in the pelitic system. *Contributions to Mineralogy and Petrology* **98,** 257–275.

Wager, L. R. & Brown, G. M. (1968). *Layered Igneous Rocks*. London: Oliver & Boyd.

Weibe, R. A. (1993). The Pleasant Bay layered gabbro-diorite, Coastal Maine: ponding and crystallization of basaltic injections into a silicic magma chamber. *Journal of Petrology* **34**, 461–489.

Wiebe, R. A. (1995). Mafic–silicic layered intrusions. In: Brown, M. & Piccoli-Phillip, M. (eds) *The Origin of Granites and Related Rocks*. Reston, VA: US Geological Survey.

Wilcox, R. E. (1954). Petrology of Parícutin volcano, Mexico. *Geological Survey Bulletin* **965-C,** 281–353.

Wilson, J. R. & Engel-Sørensen, O. (1986). Basal reversals in layered intrusions are evidence for emplacement of compositionally stratified magma. *Nature* **326,** 616–618.

Wilson, J. R. & Sørensen, H. S. (1996). The Fongen–Hyllingen layered intrusive complex, Norway. In: Cawthorn, R. G. (ed.) *Layered Intrusions. Developments in Igneous Petrology 15*. Amsterdam: Elsevier, pp. 303–330.

Wilson, J. R., Menuge, J. F., Pedersen, S. & Engel-Sørensen, O. (1987). The southern part of the Fongen–Hyllingen layered mafic complex, Norway: emplacement and crystallization of compositionally stratified magma. In: Parsons, I. (ed.) *Origins of Igneous Layering*. Dordrecht: Reidel, pp. 145–185.